Astronomy & Astrophysics

Neutral gas in Lyman-alpha emitting galaxies Haro 11 and ESO 338-IG04 measured through sodium absorption[★]

A. Sandberg[1], G. Östlin[1], M. Hayes[2,3], K. Fathi[1], D. Schaerer[4,3], J. M. Mas-Hesse[5], and T. Rivera-Thorsen[1]

[1] The Oskar Klein Centre, Department of Astronomy, Stockholm University, AlbaNova, 106 91 Stockholm, Sweden
  e-mail: sandberg@astro.su.se
[2] Université de Toulouse, UPS – OMP, IRAP, 31028 Toulouse Cedex 04, France
[3] CNRS, IRAP, 14 avenue Edouard Belin, 31400 Toulouse, France
[4] Observatoire de Genève, Université de Genève, 51 Ch. des Maillettes, 1290 Versoix, Switzerland
[5] Centro de Astrobiología (CSIC–INTA), 28850 Madrid, Spain

ABSTRACT

Context. The Lyman alpha emission line of neutral hydrogen is an important tool for finding galaxies at high redshift, thus for probing the structure of the early universe. However, the resonance nature of the line and its sensitivity to dust and neutral gas is still not fully understood.
Aims. We present measurements of the velocity, covering fraction and optical depth of neutral gas in front of two well-known, local blue compact galaxies that show Lyman alpha in emission: ESO 338-IG 04 and Haro 11. We thus observationally test the hypothesis that Lyman alpha can escape through neutral gas by being Doppler shifted out of resonance.
Methods. We present integral field spectroscopy, obtained with the GIRAFFE/Argus spectrograph at VLT/FLAMES in Paranal, Chile. The excellent wavelength resolution allowed us to accurately measure the velocity of the ionized and neutral gas through the Hα emission and Na D absorption, which trace the ionized medium and cold interstellar gas, respectively. We also present independent measurements from the VLT/X-shooter spectrograph that confirm our results.
Results. For ESO 338-IG04 we measure no significant shift of neutral gas: the best fit velocity offset is -15 ± 16 km s^{-1}. For Haro 11, we see an outflow from knot B at 44 ± 13 km s^{-1}, and infalling gas towards knot C with 32 ± 12 km s^{-1}. Based on the relative strength of the Na D absorption lines, we estimate low covering fractions of neutral gas (down to 10%) in all three cases.
Conclusions. The Na D absorption most likely occurs in dense clumps with higher column densities than the medium in which the bulk of the Ly α scattering takes place. Still, we find no strong correlation between outflowing neutral gas and strong Ly α emission. The Ly α photons from these two galaxies are therefore likely to be escaping due to a low column density and/or covering fraction.

Key words. galaxies: kinematics and dynamics – galaxies: ISM – galaxies: starburst – galaxies: individual: Haro 11 – galaxies: individual: ESO 338-IG04

1. Introduction

The Lyman alpha (Ly α) emission line was first suggested as a probe for discovering high redshift galaxies by Partridge & Peebles (1967). When absorbed by neutral hydrogen gas, approximately two thirds of the ionizing photons from hot, massive stars are reprocessed into Ly α photons, assuming case B recombination. The fraction of the bolometric flux reprocessed in the Ly α line could therefore be as high as six to seven per cent in a young, star-forming population. However, early surveys designed for finding Lyman alpha emitting galaxies (LAEs) came up blank. (see e.g. Pritchet 1994, and references therein).

It was only with deeper and larger surveys (e.g. Cowie & Hu 1998) that targeting Ly α became the successful method that it is today for finding galaxies at redshifts $z \gtrsim 2$. It has since been widely used for mapping out the large-scale structure of the high-redshift universe (e.g. Rhoads et al. 2000; Kudritzki et al. 2000; Malhotra & Rhoads 2002; Ouchi et al. 2003, 2005; Gawiser et al. 2006; Ajiki et al. 2006; Gronwall et al. 2007; Pirzkal et al. 2007; Finkelstein et al. 2008; Nilsson et al. 2009; Yuma et al. 2010; Ouchi et al. 2010; Guaita et al. 2011; Adams et al. 2011; Blanc et al. 2011; Shibuya et al. 2012) and even for

constraining the epoch of cosmic reionization (e.g. Malhotra & Rhoads 2004; Dijkstra et al. 2007; Ono et al. 2010; Jensen et al. 2013).

As shown by Hayes et al. (2010), up to 90 percent of star-forming galaxies in high-redshift surveys emit too little Ly α to be detected by standard criteria. The earliest candidate to be blamed for this apparent discrepancy between theory and observation was absorption by dust, which is strongest in the ultraviolet. Early surveys in the local Universe hinted at an anti-correlation between the metallicity (which generally correlates with dust content) and Ly α luminosity (e.g. Meier & Terlevich 1981), but it soon became clear that dust alone could not explain the deviation from recombination theory (Giavalisco et al. 1996). In particular one galaxy, I Zw 18, shows a very low metallicity combined with strong Ly α absorption (Kunth et al. 1994).

Attention was then turned to resonant scattering of Ly α in H I, which had been explored theoretically for a time (e.g. Osterbrock 1962; Adams 1972). If the path length of Ly α photons is greatly increased in multiple scatterings, even small amounts of dust can cause strong absorption (Neufeld 1990). However, if the neutral gas is shifted in velocity, the Ly α photons are shifted out of resonance and can escape from the galaxy more easily. Kunth et al. (1998) showed from a sample of eight local gas-rich dwarf galaxies that the emission of Ly α in each

case exhibited a P Cygni profile, accompanied by blueshifted absorption in the low ionization-stage metal lines. This suggests that an outflow of neutral gas would allow the Ly α emission to escape more easily along the line-of-sight. Modern simulations (e.g. Verhamme et al. 2006; Garel et al. 2012; Duval et al. 2013) thus take a combination of the relative velocities of ionized and neutral hydrogen gas into account, as well as dust, and their respective distributions, all of which may influence the escape of Ly α from galaxies.

Although neutral gas is best traced through LIS absorption lines in the UV, such a study at low redshift requires a space telescope because of ultraviolet absorption in the atmosphere. The current options for this are either HST/STIS, which has a low sensitivity, or HST/COS with limited spatial information. However, the emission and absorption of Ly α may vary on small scales (Mas-Hesse et al. 2003; Östlin et al. 2009) and a detailed study requires some degree of spatial resolution. It is therefore advantageous to identify an alternative set of longer wavelength absorption features that still form in the neutral ISM, in order to facilitate the use of contiguous integral field spectrographs attached to large-aperture telescopes on the ground. Neutral gas motions in star-forming galaxies have been studied in the past using, e.g. the Mg $\textsc{ii}\lambda\lambda2796,2803$Å doublet (e.g. Churchill & Vogt 2001; Mshar et al. 2007; Martin & Bouché 2009; Nestor et al. 2011) and Na $\textsc{i}\lambda\lambda5889,5895$ (e.g. Heckman et al. 2000; Rupke et al. 2002; Martin 2005; Chen et al. 2010), although never before have such kinematic tracers been used with reference to Ly α.

In this paper, we present the first spatially resolved study of absorption from Na $\textsc{i}$ in the cold interstellar gas in two nearby Ly α emitting blue compact galaxies. Specifically, we target the sodium resonance absorption doublet ($\lambda\lambda$ 5889.95,5895.92), which we will refer to as Na D in this paper. The galaxies are Haro 11 (ESO 350-IG38) and ESO 338-IG04 (Tololo 1924-416) which are both objects of intense study due to their Ly α emission and possible similarities to LAEs and Lyman Break Galaxies (LBGs) at high redshift (see Sect. 2).

Na D is generally stronger than other resonance lines in the optical (such as K $\textsc{i}$ or Ca $\textsc{ii}$, which are strongly depleted in diffuse, low-velocity clouds, see e.g. Spitzer 1968). With an ionization potential of 5.14 eV it is a good tracer of neutral hydrogen. By simultaneously studying the Hα emission line, we can accurately determine the location, extent and velocity distribution of the ionized hydrogen in these galaxies. We are thus able to measure the relative velocities between the ionized and neutral media, which is precisely the Doppler shift relevant for Ly α transmission. With integral field unit spectra from Argus at VLT/FLAMES we achieve a high spectral resolution combined with spatial information. We include an independent measurement from VLT/X-shooter that confirms these results, and enables us to estimate the stellar contamination of the interstellar Na D absorption.

The paper proceeds as follows; in Sect. 2 we describe previous studies of the two galaxies in our sample in more detail. In Sect. 3 we describe our data and the reduction steps. In Sect. 4 we present our results. In Sect. 5 we discuss possible complications from stellar contamination. In Sect. 6 we discuss our results, and in Sect. 7 we leave our concluding remarks.

2. Sample

For various reasons, the two galaxies in our sample have already been studied extensively, but the neutral gas velocity as estimated from the sodium doublet has not yet been measured

with either high precision or spatial resolution. Analyzing VLT/UVES spectra of ESO 338-IG04, Östlin et al. (2007) estimated an outflow velocity ~20 km s^{-1} from Na D, but emphasized that with their low signal to noise data they could not disentangle the relative contributions of stellar and ISM absorption.

HST UV imaging of the two galaxies (Kunth et al. 2003; Hayes et al. 2005, 2007; Östlin et al. 2009) gives us information on the Ly α and UV continuum morphologies. Haro 11 is a blue compact galaxy at $z = 0.02$ with three main condensations or "knots". The knots are traditionally called A, B and C (Vader et al. 1993), as shown in the left panel of Fig. 1. Knot C appears to be the brightest knot in the ultraviolet and also shows Ly α in emission, while knot B is brightest in Hα but instead shows Ly α in absorption. These two knots are therefore of particular interest as laboratories in which we try to explain why Ly α is emitted from one but absorbed in the other. Evidence suggests that Haro 11 is the result of a dwarf galaxy merger (Östlin et al. 2001), particularly because of the irregular morphology, the high relative velocities between the knots of several hundred km s^{-1}, the broad emission lines, and the presence of a tidal arm structure with a high redshifted velocity relative to the rest of the system (Östlin et al. 2013, in preparation). The H α line width within a star forming knot is as high as ~270 km s^{-1} (FWHM), and shows strong multi-component features.

Kunth et al. (1998) present HST/GHRS spectra of Haro 11 around Ly α and the interstellar O $\textsc{i}$ (λ1302Å) and Si $\textsc{ii}$ (λ1304Å) lines, estimating an outflow velocity of the neutral medium of around 60 km s^{-1}. Both absorption lines are very broad, indicating multiple components along the line-of-sight, spanning roughly 200 km s^{-1}. The Ly α line profile has a strong underlying absorption, extending more than 1500 km s^{-1} on the blue side of the emission. The line does not show a clear P Cygni profile, and the underlying absorption seems to extend also to the red side. Evidence for several blueshifted Ly α components was found, indicating multiple absorbing gas clouds. Unfortunately, it is not clear exactly where in the galaxy the $1\farcs7 \times 1\farcs7$ GHRS aperture was pointed (see discussion in Hayes et al. 2007).

ESO 338-IG04 has slightly narrower emission lines than Haro 11 (*FWHM* $\sim$ 180 km s^{-1}) and the Ly α emission is concentrated to a bright central region. ESO 338-IG04 is riddled with "super star clusters"; small knots of intense star formation (Östlin et al. 1998, 2003, 2007). The ongoing starburst is about 40 Myr old and was probably triggered by a merger with a small galaxy or from an interaction with remaining debris from a previous encounter with the companion galaxy ESO 338-IG04b (Östlin et al. 2001; Cannon et al. 2004). When we discuss ESO 338-IG04 below, we mainly focus on the bright central region, which we refer to as knot A (Hayes et al. 2005, cf. Fig. 1; also known as cluster # 23 in the "inner" sample of Östlin et al. 1998).

Hayes et al. (2005) present a detailed description of a HST/STIS long-slit spectrum across ESO 338-IG04. The spectrum shows diffuse Ly α emission in several regions, but over knot A the Ly α emission is weak and shows only a hint of blueshifted absorption. However, the low resolution of the spectrum makes a detailed kinematical study difficult, and the emission line lies very close to the strong geocoronal Ly α line. The slit is also only $0\farcs2$ wide, and was not optimally centered over knot A. It is therefore not clear how well this spectrum samples the Ly α profile in this region. An outflow velocity from this STIS spectrum was estimated by Schwartz et al. (2006) from low ionization state absorption lines to be 47 ± 70 km s^{-1}.

In this paper we look mainly at the strong knots in the respective galaxies; the positions of our chosen spectroscopic analysis
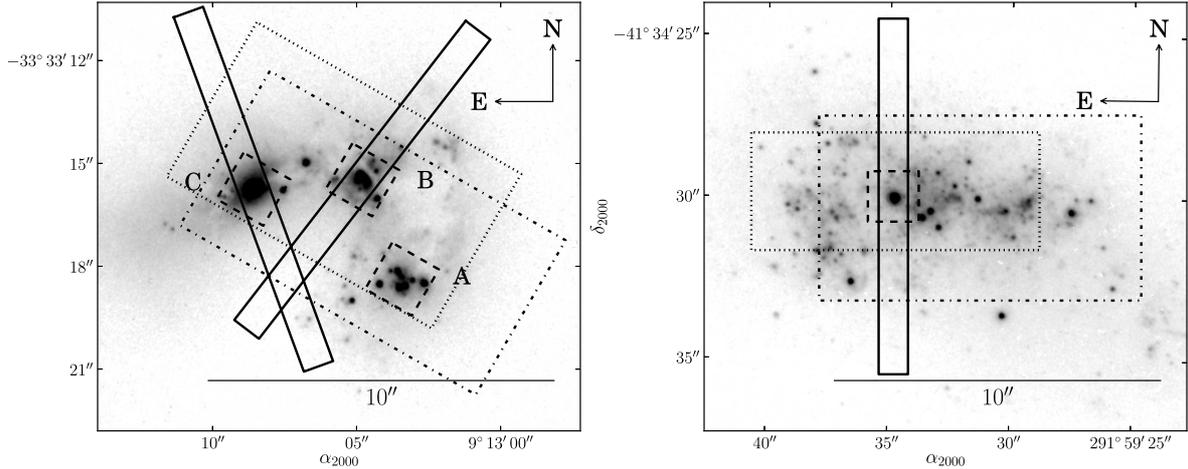
Fig. 1. Slit positions, field of view (FOV) and approximate aperture positions for Haro 11 (*left*) and ESO 338-IG04 (*right*), overlayed on HST/ACS F550M continuum images (i.e. close in wavelength to the Na D feature). The X-shooter slits are 0.9 (or 1.0 for the UVB-arm, not marked in the figure) arcsec wide and 11 arcsec long and marked with solid lines. The FOV for the LR6 setting (which includes Hα) is marked with dash-dotted lines while the shorter LR5 setting (including Na D) is marked with dotted lines. The Argus binned "apertures" are 1.56 arcsec wide squares marked with dashed lines. The VLT/FLAMES FOV shown here shows the area for which we have full exposure after taking into account the dithering.

windows are shown in Fig. 1. Even though our field of view with VLT/FLAMES is large, the Na D signature is very weak and the areas marked are the only regions in which we can successfully fit the Na D lines, even after spatially binning our data.

3. Observations and data reduction

3.1. Integral field spectroscopy with VLT/FLAMES

The integral field spectroscopy observations (ESO ID 083.B-0470(A)) were performed between June 9 and July 6 2009 with the Argus integral field unit of the GIRAFFE spectrograph at the FLAMES instrument at VLT/UT2. Argus consists of 14 × 22 lenslets arranged in a rectangular grid, giving to a field-of-view of approximately 7 × 11 arcsec. Each lenslet is then fed to the spectrograph by a fiber, yielding a spectrum for each lenslet.

We observed the two galaxies with two "low resolution" ($\mathcal{R} = 11\,800-13\,700$) gratings. The LR6 grating (which covers $\lambda\ 6438-7184$ Å) was used to observe the Hα emission line ($\lambda\ 6562.82$ Å), and the LR5 grating ($\lambda\ 5741-6524$ Å) for the Na D doublet ($\lambda\lambda\ 5889.95, 5895.92$ Å). The exposure times for both galaxies were 8×195 s = 1560 s in the LR6 grating, and 12×895 s + 2×915 s = 12 570 s in LR5. The seeing (recorded from the DIMM telescope) varied between 0″.5 and 0″.8 for both LR5 observations; for LR6 it was ~0″.8 for Haro 11 and 0″.9−1″.3 for ESO 338-IG04.

Basic bias and flatfield corrections, wavelength calibrations and sky subtractions were performed with recipes from the common pipeline library (CPL) package version 5.2.0 in `esorex`. The bias frames were median combined with the `gimasterbias` recipe, producing master bias frames for each observing night. The `gimasterflat` recipe was then used for calibrating the fiber positioning onto the CCD. The flatfield frames used for each observing block were always acquired during the same night, using the Nasmyth screen (which gives better illumination in Argus mode). The `giwavecalibration` recipe subsequently performs the wavelength calibration by mapping known wavelengths from a calibration lamp. This recipe requires an existing dispersion solution as an initial guess, which is then refined. We checked the convergence of this procedure by giving

the refined dispersion solution as a new initial guess and ensuring that the two refined solutions were identical for each calibration set. Finally, the `giscience` recipe was used to apply all calibrations to the data, and create a data cube with two spatial dimensions and one spectral.

Each science spectrum was reduced individually. As a sanity check, we verify the sky subtraction by measuring the continuum flux in regions far from the bright condensations, which we find to be consistent with zero.

The subsequent reduction steps were made with the PyFITS module version 2.3.1 for Python[1]. Since the science data were dithered (the telescope made small movements of roughly 0.5 to 1 arcsec between each science exposure), we created an empty (x, y, λ) cube with spatial dimensions matching those of the region corresponding to the region on the sky for which we had contributions from each science exposure. The spectral data were then combined onto this grid using a weighted average intensity for each integral field unit pixel (or "spaxel"), calculated from the uncertainties obtained from the pipeline. The dithering shifts were rounded off to whole spaxels before combining. This may thus introduce a small astrometric shift of up to 0″.25 in an individual exposure. Our final spatial resolution is therefore expected to be similar to our worst seeing of about one arcsec. The final data product has the original 0″.52/lenslet spatial sampling, and 0.2 Å spectral resolution. In this paper we always consider combined spaxels in a 3x3 configuration, corresponding to a bin size of 1″.56.

Line profiles where fitted using the optimize.leastsq routine from the Scipy[2] version 0.7.0 Python package, which uses a Levenberg-Marquardt least-squares minimization technique.

3.2. VLT/X-shooter spectra

The X-shooter data were obtained as part of the first science verification for the instrument between August 10 and 11, 2009 (ESO ID 60.A-9433(A)). For the VIS arm ($\lambda \sim 5500-10\,200$), a slit of 0″.9 × 11″ was used. For the UVB arm ($\lambda \sim 3000-5600$),

---

[1] PyFITS is a product of the Space Telescope Science Institute, which is operated by AURA for NASA.
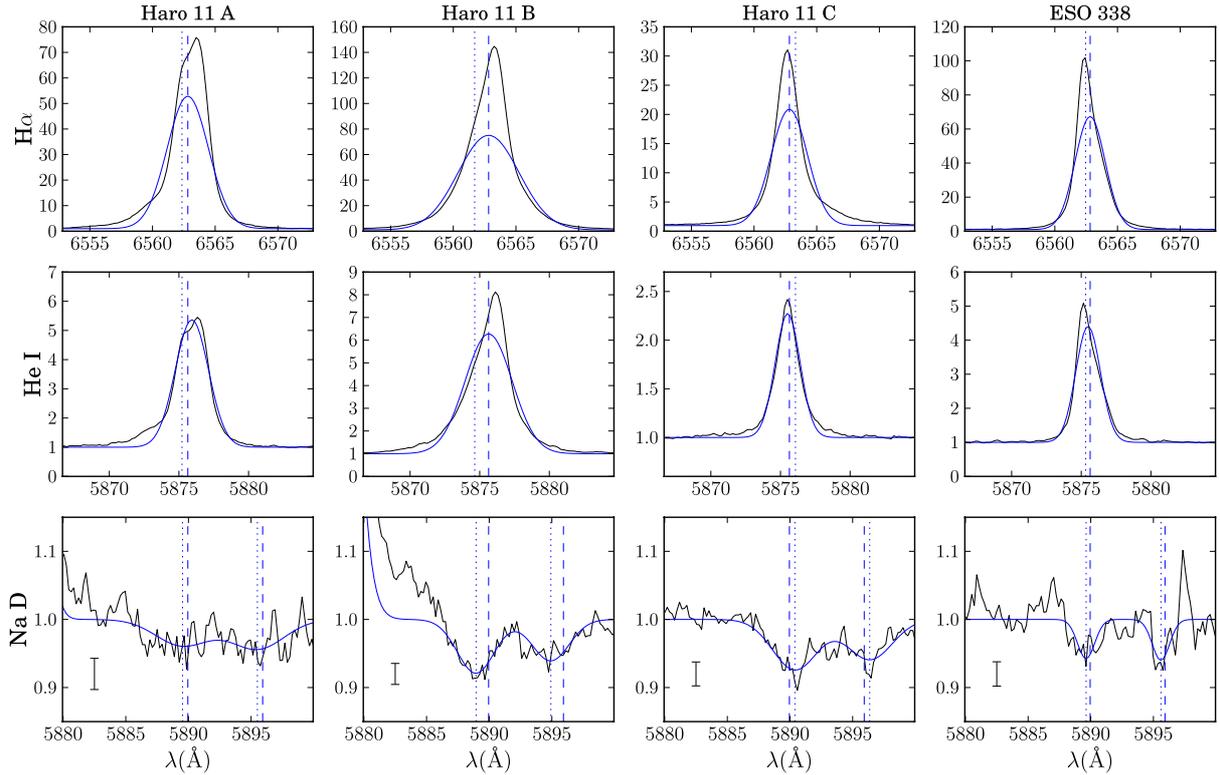
[2] http://www.scipy.org

Fig. 2. Hα, He I (5875.6) and Na D line profiles from the VLT/FLAMES data. The blue Gaussians are a simple fit to the emission or absorption lines. In the case of Haro 11 knot A, the best fit is shown in this figure but is never used. The vertical dashed lines show the velocity given by the Hα Gaussian fit, and the vertical dotted lines show the Na D velocity. The y-axis is normalized to the continuum. Also shown inset in the *bottom row* are errorbars, representing the standard deviation in the continuum from 5900 to 5950 Å, which shows no emission or absorption features. Since the spectra are normalized to the continuum, these errorbars reflect the strength of the continuum in each region.

the slit was $1'' \times 11''$. The resolving power $\mathcal{R}$ is 8800 and 5100 for the VIS and UVB arms, respectively.

The spectra were reduced with the X-shooter pipeline v. 1.3.7 using `esorex` v. 3.9.0. Standard settings were used in the physical model mode, using the `xsh_scired_slit_nod` recipe to perform reduction, sky subtraction and extraction of the science frames.

These data are also analyzed by Guseva et al. (2012), but we have included different reduction steps and we do not discuss the data from the NIR arm. With the large wavelength range of these data, we can examine the effect of the underlying photospheric Balmer absorption on the Hα emission feature. It is strongest in ESO 338-IG04, but negligible for our discussion in all cases.

4. Results

The Na D feature is very weak in these galaxies and we were therefore forced to bin our FLAMES spectra in the spatial dimension. Even in this case, only the very strongest continuum features show Na D absorption. This reduces our discussion of the larger fields of view of FLAMES to the selected binned apertures shown in Fig. 1. Except for knot A in Haro 11, these are the only regions where we can see a clear Na D absorption profile. Nevertheless, these apertures still allow us to perform a sufficiently detailed analysis in some of the most interesting Ly α emitting and absorbing regions.

The most important spectral features from the apertures are shown in Fig. 2. The spectra are not flux calibrated and are instead shown normalized to the continuum. The continuum was in all cases fitted with a low-order polynomial across the

Table 1. X-shooter observing specifications.

Parameter	Haro 11B	Haro 11C	ESO 338-IG04
Airmass	1.016	1.012	1.430
Seeing	0''7	0''7–1''3	0''6
Exposure time	800 s	680 s	600 s

entire observed range, which yielded a good fit. The Hα and He I (5875.64 Å) lines both show strong multi-component features, as is evident from the deviation from a simple Gaussian. Note that these features are very similar in both emission lines. We verify that the asymmetry is not an instrumental feature by examining the shape of skylines and of calibration lamp frames. The measured velocities of the different spectral components are listed in Table 3.

We have also attempted multiple-component fits to the Hα emission lines (not shown). In all cases, we identify two strong components: one narrow "main" component and one broader but weaker one. In the case of Haro 11 B and ESO 338-IG04, the velocity of the broad component is consistent with the velocity of the main component, within the uncertainties. For Haro 11 A the narrow (broad) component has a velocity of 6242±7 (6189±10), and it is clear that the profile is very complex, but we have no good Na D against which to compare. In the case of Haro 11 C the weak, broad component is centered roughly at the same velocity as the Na D profiles. In this case, the contribution to the Ly α flux from this component is therefore not only expected to be weaker intrinsically, but should also suffer stronger resonance absorption. In each case, these secondary
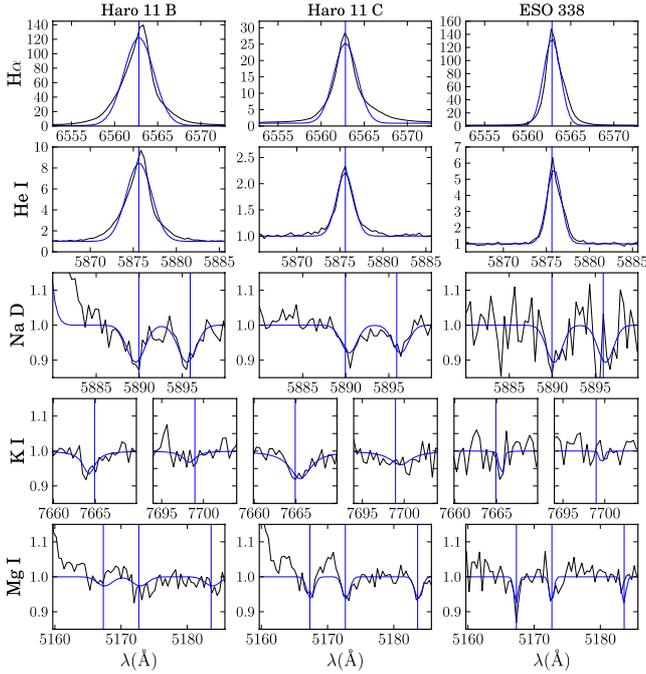
Fig. 3. Hα, He I (5875.6), Na D, K I and Mg I line profiles from the VLT/X-shooter data. The blue Gaussians are a simple fit to the emission or absorption lines. The vertical lines show the systemic velocity as given by the Hα Gaussian fit. The y-axis is normalized to the continuum.

components do not change the velocity of the main component by more than a few km s^{-1}, and for simplicity we have chosen not to include them in the further discussion. Our goal is not to perfectly reproduce the line shapes but to analyze the velocities of the main constituents of the galaxies. We note that the components we measure in Haro 11 agree well with the recent results from James et al. (2013).

We also attempted a simple wavelength centroid fit, numerically defined as $\Sigma\lambda f_\lambda/\Sigma f_\lambda$, across the continuum-subtracted emission lines. The result is fully consistent with the numbers we use in this paper, with a maximum shift in velocity of 5 km s^{-1}.

The X-shooter spectra are shown for comparison in Fig. 3 (see also Sect. 5). Note that single Gaussian fits appear to reproduce the line shapes better for these data, but this is mainly due to the lower spectral resolution and signal-to-noise.

We see the velocity of emission lines from ionized gas are the same within each region we measure, independent of the species used. In the same region, the velocities as measured by the emission lines of Hα (λ 6562.8 Å), He I (λ 5875.6 Å), [O I] ($\lambda\lambda$ 6300.2, 6363.9 Å), [N II] ($\lambda\lambda$ 6548.1, 6583.6 Å), and [S II] ($\lambda\lambda$ 6716.5, 6730.7 Å) are all the same, within uncertainties.

In general, the Na D features are weak in both galaxies. For Haro 11, we measure an equivalent width for the doublet of $EW_{NaD} = -0.42 \pm 0.06$ Å for knot C, -0.36 ± 0.06 Å for knot B, and -0.15 ± 0.04 Å for ESO 338-IG04. For Haro 11 A we estimate an upper limit of -0.15 Å. These values are estimated purely from the FLAMES spectra. The ratios between the EW of the separate lines of the doublet are close to unity (cf. Table 2), which indicates a high optical depth in the individual clouds along the sightlines where the absorption occurs. Note, however, that this is not the same as the average optical depth along all sightlines in the aperture, which is clearly smaller. The Na D line ratio in the optically thin case is 2:1. In Table 2 we present the

Table 2. Na D properties and dust extinction.

Parameter	Haro 11B	Haro 11C	ESO 338-IG04
Na D doublet EW (Å)	-0.36 ± 0.06	-0.42 ± 0.06	-0.15 ± 0.04
Na D 5890/5896 ratio	1.15 ± 0.22	1.14 ± 0.18	0.94 ± 0.47
Na D optical depth	>2	>2	$\gtrsim 1.6$
Na D mean shift (km s^{-1})	-44 ± 13	32 ± 12	-15 ± 16
Nebular $E(B-V)$	0.42^a	0.48^a	$<0.1^b$

References. [a] Hayes et al. (2007), [b] Bergvall & Östlin (2002).

Table 3. Best fit observed velocities, in km s^{-1}.

Line	Haro11A	Haro 11B	Haro 11C	ESO 338-IG04
Hα	6227 ± 10	6146 ± 5	6126 ± 7	2859 ± 6
He I	6242 ± 9	6147 ± 6	6121 ± 9	2856 ± 11
Mg I	...	6162 ± 20	6128 ± 15	2853 ± 20
Na D	...	6102 ± 9	6158 ± 8	2844 ± 14
K I	...	6123 ± 20	6146 ± 20	2830 ± 20

Notes. Mg I and K I are measured only from VLT/X-shooter and the uncertainty is therefore larger. The other lines were measured in both VLT/FLAMES and VLT/X-shooter and this represents the weighted average.

estimated line-center optical depths of Na D, derived from the line ratio (Table 2.1 of Spitzer 1968), which are all found to be optically thick. In this regime, the covering fraction can simply be estimated as $C_f = 1 - I_{5890}$, where I_{5890} is the residual intensity in the blue Na D line. Note however, that the residual intensity may be low in narrow, unresolved components in our spectrum and that we may therefore measure an artificially stronger intensity. We will return to this point in Sect. 6.2. With this simple assumption, we estimate a lower limit to the covering fraction of Na D of ∼10% in Haro 11 knots B and C, and roughly 5% in ESO 338-IG04.

For Haro 11, we detect no measurable Na D absorption toward knot A. This is probably due to the low continuum brightness in this region which is necessary for observing absorption lines, combined with a low covering fraction of neutral gas. For knot B, we are able to measure the Na D velocity and find a moderate blueshift (compared to the ionized gas) of 44 ± 13 km s^{-1}. In knot C the absorption is stronger and we find a redshifted velocity of 32 ± 12 km s^{-1}.

In ESO 338-IG04, we are only able to measure the Na D velocity in the brightest knot (knot A), were both the continuum and the Ly α emission is strongest. We find no evidence for a shift in the velocity, with the best fit giving -15 ± 16 km s^{-1}. Östlin et al. (2007) estimated a shift of ≈20 km s^{-1} from UVES spectra with a lower signal to noise. Our estimate of the stellar versus nebular velocity agrees well with the analysis of Cumming et al. (2008), where the stellar component (as measured by the Ca II triplet ($\lambda\lambda$ 8498, 8542, 8662 Å) shows the same velocity as the nebular gas, with a value of 2860 ± 4 km s^{-1}.

5. Possible stellar contamination of Na D

A challenge with using Na D to measure neutral gas flows is that the stars in the galaxy may also exhibit the absorption lines. In this section we demonstrate that the Na D we measure is primarily of interstellar origin.

Na D is prominent in spectra of cool stars: K- and M-type giants and supergiants. There are several ways of disentangling

the stellar and interstellar sodium. One of the more common and robust methods make use of the Mg I b-band triplet ($\lambda\lambda$ 5167.32, 5172.68, 5183.60 Å). It has a very similar ionization potential as Na, and the two elements are formed under similar conditions in stars. However, the triplet forms between excited states and is not found in the cold, neutral medium. Therefore, any detection of Mg I b must come from stellar atmospheres.

Thanks to their similar origins, the equivalent widths of the Mg b triplet and the stellar Na D doublet are strongly correlated. However, any ground-based spectra of nearby stars are always contaminated by telluric Na D emission, which makes the ratio difficult to measure. Rupke et al. (2002) compiled measurements of Galactic globular clusters and mostly non-active galaxies (Bica & Alloin 1986) and nuclei of nearby galaxies (Heckman et al. 1980). They found the equivalent widths of the purely stellar features to be correlated as $EW_{NaD} \sim 0.5\,EW_{Mg\,b}$, with a possible intrinsic scatter of $\gtrsim 25\%$. Heckman et al. (2000) combined the data from Heckman et al. (1980) with stellar library data from Jacoby et al. (1984), and estimated $EW_{NaD} \sim 0.75\,EW_{Mg\,b}$, which agrees with their own K giant spectra to within 0.10 dex. Schwartz & Martin (2004) also make a fit to the data by Jacoby et al. (1984) to find $EW_{NaD} = 0.40 \pm 0.05\,EW_{Mg\,b}$. Martin (2005) analyzed Keck II/ESI spectra of A, F, G and K dwarfs and giants and concluded $EW_{NaD} = 1/3\,EW_{Mg\,b}$ and that the stellar contribution was consistently less than 10% in their study of 18 Ultra Luminous Infrared Galaxies. Sato et al. (2009) investigate Na D absorption in 493 spectra from the AEGIS survey, and find $EW_{NaD} = 0.40\,EW_{Mg\,b}$ well describes the purely stellar boundary in their sample (see their Fig. 1). Finally, Chen et al. (2010) used Sloan Digital Sky Survey (SDSS) spectra from young disc galaxies and estimate that an average $\sim$80% of the Na D absorption arises in stellar atmospheres. Their estimate of the stellar contribution is based on fitting and subtracting a stellar population synthesis model to the continuum and absorption features, and they emphasize that their spectral model sometimes shows stronger Na D absorption than the actual data. They conclude that the most likely explanation is that Na D is sometimes seen in emission in their data, predominantly from face-on galaxies with low dust attenuation. This is because a stronger underlying stellar contamination is expected in the spectra of normal star-forming galaxies compared to younger stellar populations (i.e. ones more akin to the young populations of our two blue compact galaxies).

We note that Na D is a resonance absorption feature, and therefore absorbed photons will be re-emitted in a random direction. This can create a diffuse, low surface brightness emission component. Prochaska et al. (2011) model the effect of re-emitted light and conclude that in the extreme case that all of this light eventually escapes and is caught within the aperture, it can significantly reduce the observed equivalent width. We expect this effect to be very small in our analysis, however, since we are looking only at narrow slits and apertures that are small compared to the galaxies (1.5 arcsec corresponds to roughly 0.6 kpc in Haro 11 and just 0.3 kpc in ESO 338-IG04).

An alternative to measuring outflows with Na D is the K I doublet ($\lambda\lambda$ 7664.91, 7698.97 Å). With similar properties and a similar ionization potential of 4.34 eV (compared to 5.14 eV for Na D), these lines are expected to behave much in the same way (see e.g. Kemp et al. 2002). They are used very seldom, however, because Na D is typically stronger, and also because they often overlap with atmospheric O_2 absorption bands.

We use our X-shooter data to estimate the stellar contamination. Due to the comparatively low signal-to-noise and lower resolution of the X-shooter data, the equivalent widths are not as easily determined as for the Argus data. However, we can still use our spectra in Fig. 3 to see that it is only in Haro 11 C that we can clearly see the Mg b feature, although it is still very weak. We thus take the upper limit from Haro 11 C as the upper limit on the stellar contamination for all our results. If the EW of Mg b was larger than this limit in the other regions, it would be readily seen in Fig. 3. We estimate the EW of this feature to be roughly -0.2 Å, i.e. about half the equivalent width of Na D.

Based on the discussion above we estimate the stellar contribution to be on the order of 25–30%, but we note that it may be as high as 50% in the extreme case. A significant contribution to the Na D profile at the stellar velocity (which is consistent with the H-alpha velocity in our galaxies) would decrease the average offset velocities that we measure. The absolute value of our Na D velocities may therefore be somewhat lower, if anything, than the purely nebular Na D velocity.

6. Discussion

We have measured outflow/inflow velocities and covering fractions of the neutral ISM in front of three bright star-forming condensations, two of which show Ly α emission (ESO 338-IG04 A, and Haro 11 C) and one shows Ly α in absorption (Haro 11 B). We also compile measurements of the nebular dust attenuation in these regions from our previous investigations: Hayes et al. (2007) for Haro 11, Bergvall & Östlin (2002) for ESO 338-IG04, see Table 2.

6.1. Comments on the individual regions

Emission – ESO 338-IG04 knot A. For ESO338-IG04, we find that the velocity of the neutral gas (as estimated from the Na D absorption) is only very slightly blueshifted (or even static) compared to the ionized gas. This would rule out the outflow scenario as an explanation for the observed direct Ly α escape from this region. However, we note that Hα from the central region (knot A) of ESO 338 is dominated by a large H II shell (Bergvall & Östlin 2002). The UVES spectra analyzed by Östlin et al. (2007) show a multi-component feature in the [O III] (λ5007 Å) and Hα lines towards knot A, which they interpret as an expanding bubble with a velocity of $\sim$40 km s^{-1}. Presumably this shell is made from outflowing ionized gas produced by stellar winds and supernovae, yet we measure a low outflow velocity in H I. If there is indeed an expanding ionized bubble in ESO 338-IG04, it is possible that the Hα feature is dominated by emission on the side of the bubble facing our way. This would cause us to measure a more blueshifted velocity for the ionized gas and reduce our inferred neutral gas velocity shift. However, the bubble seems to be optically thin, which would mean that the effect is very small, and also the stellar component in knot A appears to have the same velocity as the ionized gas (Cumming et al. 2008).

Emission – Haro 11 knot C. For Haro 11, we find a small redshifted velocity of Na D in front of knot C, indicating infall of cold gas. HST imaging shows Ly α emission from this region, which could partially result from this velocity difference. However, it is in the opposite direction to the outflow that would be expected from the Ly α profile, and the velocity shift is also rather modest.

There is evidence for a dust-corrected Lyα/Hα ratio higher than the case B recombination value in both ESO 338-IG04 A (Östlin et al. 2009) and Haro 11 C (Atek et al. 2008). This could

in principle be due to Ly α photons actually suffering less attenuation than the continuum as they scattering on the surface of cool dusty clumps (Neufeld 1991), although recent simulations (Laursen et al. 2012; Duval et al. 2013) suggest this scenario to be unlikely. It is also possible that an attenuation correction based on a clumpy dust distribution (rather than a uniform screen) could reconcile the line ratios with their intrinsic recombination values (Scarlata et al. 2009).

Absorption – Haro 11 knot B. For knot B, we find a moderate blueshifted velocity. Combined with a low covering fraction of ~10%, Ly α should escape more easily from knot B. However, our HST imaging shows that Ly α is strongly absorbed in this region.

There is some debate as to whether the dust extinction is higher in knot B than in knot C. Judging from HST images, there do seem to be more dust clouds near and around knot B, and based on the X-shooter data knot C has a lower extinction (Guseva et al. 2012). However, the Hα and Hβ images from which we derive the $E(B-V)$ values presented in Table 2 give approximately the same level of extinction in both knots (Hayes et al. 2007; Atek et al. 2008). If the medium is highly clumpy it is likely that the extinction varies along different sightlines in the aperture, even over these small regions. Inconsistent results may therefore be expected because of different aperture sizes and positions, as well as different techniques for measuring the extinction probing varying optical depths.

Absorption – Haro 11 knot A. The signal-to-noise and the equivalent width of Na D are too small for us to safely attempt a measurement toward knot A. This is partly because the optical continuum emission near Na D is weaker than in the other knots, but it still indicates a low covering fraction of neutral gas. Knot A exhibits both Hα and UV continuum emission from ionized regions, but no significant Ly α radiation appears to escape from them.

6.2. Interpretation of the covering fractions, optical depths and velocities

In the three regions that we have identified for study in this article, we have compiled measurements of H I covering fractions, kinematics, and dust contents.

In both knot A and B in Haro 11, absorption of Ly α is seen despite a low inferred covering fraction. However, the covering fractions that we estimate from the Na D profiles are likely to only serve as lower limits, because there may be very narrow, unresolved components with lower residual intensity in our spectra. We note that the O I and Si II lines in the GHRS spectra of Kunth et al. (1998) are considerably stronger, indicating a high covering fraction of neutral gas, consistent with the strong Ly α absorption on the blue side of the line. The resolution of GHRS ($\mathcal{R} \sim 16\,000$) is not much higher than that of our Argus Na D spectra ($\mathcal{R} = 11\,800$), and would probably not explain this difference. We note also that other Na D absorption spectra in the literature often show considerably stronger lines (e.g. Heckman et al. 2000; Martin 2005). Our conclusion is that the Na D covering fraction is indeed low in these regions. The difference from the previous measurement might in part be explained by the different apertures pointing at different sightlines in an inhomogeneous ISM. The difference may also come from the lower photoionization threshold of Na D of 5.14 eV. It is thus possible that the column density of hydrogen is high enough overall to absorb Ly α but low enough that we detect Na D only in the

densest regions. The interstellar medium is known to often be very patchy, and it would not be surprising in these two galaxies with their turbulent pasts. Since Na D has to be shielded from ionizing radiation by dust (Chen et al. 2010; Murray et al. 2007), it is likely to exist only in the densest, coolest clumps.

From the optical depths we measure from the Na D line ratio, we can put a lower limit on the column density of the gas where the absorption arises. We use the relation

$$N(\text{Na I}) = \frac{\tau_1 b}{1.497 \times 10^{-15} \lambda_1 f_1} \tag{1}$$

from Spitzer (1978), where τ_1 is the central optical depth, b is the Doppler parameter (in km s^{-1}), λ_1 is the vacuum wavelength in Å, and f_1 is the oscillator strength = 0.3180, all for the weaker (red) line. With a Doppler parameter $b = FWHM/(2\sqrt{\ln 2})$ of $\gtrsim 60$ km s^{-1} for the Na D in ESO 338-IG04, a lower limit on the Na I column density is roughly $N(\text{Na I}) \gtrsim 4 \times 10^{13}$ cm^{-2}. Converting this to a hydrogen column density of course depends heavily on the Na/H abundance ratio, but using very conservative estimates based on the conversions given in Rupke et al. (2002); Murray et al. (2007) this corresponds to N(H I) above 10^{20} cm^{-2}. Ly α becomes optically thick and resonantly scatters on neutral hydrogen already at H I column densities around 10^{13-14} cm^{-2}. It would take an enormous departure from these assumptions to make the clouds optically thin. In these dense clouds, the Ly α photons would see upwards of a million optical depths, and the clouds would be self-shielding. Still, the covering fraction of these dense clouds where we see Na D is only ~0.1. Our interpretation is that the ISM in these galaxies is inhomogeneous and probably consists of column densities between these extremes. Ly α photons would then escape through regions or patches with little neutral gas, and be blocked by gas at slightly higher column densities, while we measure our velocities and covering fractions in the very densest clumps.

For Haro 11, a picket-fence model of the ISM agrees well with the detection of the Lyman continuum (Ly C, <912 Å) escape (Bergvall et al. 2006; Leitet et al. 2011), for which *only* direct paths are viable (see e.g. Heckman et al. 2001; Zastrow et al. 2011). An indirect method of estimating LyC escape from the residual residual intensity of the C II (λ 1036) line suggests that ESO 338-IG04 is also a strong candidate for LyC escape (Leitet et al. 2013), but unfortunately the redshift is too low for a direct measurement.

The question still remains why, between knots B and C in Haro 11 with their relatively similar nebular dust content, Ly α is absorbed in knot B, which shows the *larger* kinematic offset. We hypothesize on the existence of diffuse remnant H I gas with a high covering fraction towards knot B.

Our measurements of the neutral gas velocities in Haro 11 B agree rather well with the results in Kunth et al. (1998) where an outflow of ~60 km s^{-1} measured by low ionization state absorption lines was seen. However, the same spectra show Ly α in emission which would imply that some of the emission from knot C is included in the aperture as well. It is unfortunately not clear exactly where in the galaxy the HST/GHRS aperture was placed (see discussion in Hayes et al. 2007). Most likely, it was in between the knots, and it is quite likely that the different components are mixed in the spectra. Indeed, Kunth et al. (1998) see very broad absorption features (spanning roughly 200 km s^{-1}), indicating multiple absorption components.

We note that a previous measurement of the neutral gas velocity in ESO 338-IG04 was made with HST/STIS in Schwartz et al. (2006), which agrees well with our observations. The

LIS absorption features are weak and appear close to the systemic velocity. Unfortunately, the available HST/STIS spectrum for ESO 338-IG04 is not optimized for exploring the Ly α emitting region that we investigate in this paper. In light of our results, it would be very interesting to explore both Haro 11 and ESO 338-IG04 with multiple HST/COS and HST/STIS pointings to investigate the Ly α emission and absorption profiles in unprecedented spatial and spectral detail, which can be achieved by combining the two instruments.

7. Conclusions

We have presented the first spatially resolved measurements of the sodium doublet (Na D) in the two nearby Ly α emitting galaxies Haro 11 and ESO 338-IG04. Our results can be summarized as follows:

– We find an outflow of neutral gas from knot B (which shows strong Ly α absorption) and slow infall towards knot C in Haro 11. In ESO 338-IG04 we find a slow or static interstellar medium. In the two latter cases, Ly α is seen in emission. The velocities that we find for the neutral gas are not what we would have expected from standard Ly α escape scenarios. Typically, a strong outflow is assumed to allow Ly α to escape more easily.

– From the Na D line profiles we measure relatively high optical depths but small covering fractions of Na D ($\sim$10%). We estimate the minimum column density of Na D corresponding to our limits on the optical depth, and find that Na D absorption is only likely to be detected in the very densest clumps, where $N(H\,I) > 10^{20} cm^{-2}$. Since Ly α is affected by resonant scattering already at column densities of $N(H\,I) \sim 10^{13-14}$ cm^{-2}, it is likely that the direct Ly α escape seen in knot C in Haro 11 and from ESO 338-IG04 is due to a picket-fence scenario where the interstellar medium is highly inhomogeneous and consists of both dense, neutral clumps as well as ionized gas along our lines of sight.

– We see a larger kinematical offset in Haro 11 knot B than knot C, yet B shows strong Ly α absorption in contrast to the emission from C. Given the relatively similar nebular dust content of the two knots, we hypothesize the existence of a diffuse remnant H I component with a high covering fraction towards B, and a possible perpendicular outflow from C.

References

Adams, T. F. 1972, ApJ, 174, 439
Adams, J. J., Blanc, G. A., Hill, G. J., et al. 2011, ApJS, 192, 5
Ajiki, M., Mobasher, B., Taniguchi, Y., et al. 2006, ApJ, 638, 596
Atek, H., Kunth, D., Hayes, M., Östlin, G., & Mas-Hesse, J. M. 2008, A&A, 488, 491
Bergvall, N., & Östlin, G. 2002, A&A, 390, 891
Bergvall, N., Zackrisson, E., Andersson, B.-G., et al. 2006, A&A, 448, 513
Bica, E., & Alloin, D. 1986, A&A, 166, 83
Blanc, G. A., Adams, J. J., Gebhardt, K., et al. 2011, ApJ, 736, 31
Cannon, J. M., Skillman, E. D., Kunth, D., et al. 2004, ApJ, 608, 768
Chen, Y.-M., Tremonti, C. A., Heckman, T. M., et al. 2010, AJ, 140, 445
Churchill, C. W., & Vogt, S. S. 2001, AJ, 122, 679
Cowie, L. L., & Hu, E. M. 1998, AJ, 115, 1319
Cumming, R. J., Fathi, K., Östlin, G., et al. 2008, A&A, 479, 725
Dijkstra, M., Wyithe, J. S. B., & Haiman, Z. 2007, MNRAS, 379, 253
Duval, F., Schaerer, D., Östlin, G., & Laursen, P. 2013, A&A, submitted [arXiv:1302.7042]
Finkelstein, S. L., Rhoads, J. E., Malhotra, S., Grogin, N., & Wang, J. 2008, ApJ, 678, 655
Garel, T., Blaizot, J., Guiderdoni, B., et al. 2012, MNRAS, 422, 310
Gawiser, E., van Dokkum, P. G., Gronwall, C., et al. 2006, ApJ, 642, L13
Giavalisco, M., Koratkar, A., & Calzetti, D. 1996, ApJ, 466, 831
Gronwall, C., Ciardullo, R., Hickey, T., et al. 2007, ApJ, 667, 79
Guaita, L., Acquaviva, V., Padilla, N., et al. 2011, ApJ, 733, 114
Guseva, N. G., Izotov, Y. I., Fricke, K. J., & Henkel, C. 2012, A&A, 541, A115
Hayes, M., Östlin, G., Mas-Hesse, J. M., et al. 2005, A&A, 438, 71
Hayes, M., Östlin, G., Atek, H., et al. 2007, MNRAS, 382, 1465
Hayes, M., Östlin, G., Schaerer, D., et al. 2010, Nature, 464, 562
Heckman, T. M., Crane, P. C., & Balick, B. 1980, A&AS, 40, 295
Heckman, T. M., Lehnert, M. D., Strickland, D. K., & Armus, L. 2000, ApJS, 129, 493
Heckman, T. M., Sembach, K. R., Meurer, G. R., et al. 2001, ApJ, 558, 56
Jacoby, G. H., Hunter, D. A., & Christian, C. A. 1984, ApJS, 56, 257
James, B. L., Tsamis, Y. G., Walsh, J. R., Barlow, M. J., & Westmoquette, M. S. 2013, MNRAS, accepted [arXiv:1301.1288]
Jensen, H., Laursen, P., Mellema, G., et al. 2013, MNRAS, 428, 1366
Kemp, S. N., Bates, B., Beckman, J. E., et al. 2002, MNRAS, 333, 561
Kudritzki, R.-P., Méndez, R. H., Feldmeier, J. J., et al. 2000, ApJ, 536, 19
Kunth, D., Lequeux, J., Sargent, W. L. W., & Viallefond, F. 1994, A&A, 282, 709
Kunth, D., Mas-Hesse, J. M., Terlevich, E., et al. 1998, A&A, 334, 11
Kunth, D., Leitherer, C., Mas-Hesse, J. M., Östlin, G., & Petrosian, A. 2003, ApJ, 597, 263
Laursen, P., Duval, F., & Östlin, G. 2012, ApJ, submitted [arXiv:1211.2833]
Leitet, E., Bergvall, N., Piskunov, N., & Andersson, B.-G. 2011, A&A, 532, A107
Leitet, E., Bergvall, N., Hayes, M., Linné, S., & Zackrisson, E. 2013, A&A, in press, DOI: 10.1051/0004-6361/201118370
Malhotra, S., & Rhoads, J. E. 2002, ApJ, 565, L71
Malhotra, S., & Rhoads, J. E. 2004, ApJ, 617, L5
Martin, C. L. 2005, ApJ, 621, 227
Martin, C. L., & Bouché, N. 2009, ApJ, 703, 1394
Mas-Hesse, J. M., Kunth, D., Tenorio-Tagle, G., et al. 2003, ApJ, 598, 858
Meier, D. L., & Terlevich, R. 1981, ApJ, 246, L109
Mshar, A. C., Charlton, J. C., Lynch, R. S., Churchill, C., & Kim, T.-S. 2007, ApJ, 669, 135
Murray, N., Martin, C. L., Quataert, E., & Thompson, T. A. 2007, ApJ, 660, 211
Nestor, D. B., Johnson, B. D., Wild, V., et al. 2011, MNRAS, 412, 1559
Neufeld, D. A. 1990, ApJ, 350, 216
Neufeld, D. A. 1991, ApJ, 370, L85
Nilsson, K. K., Tapken, C., Møller, P., et al. 2009, A&A, 498, 13
Ono, Y., Ouchi, M., Shimasaku, K., et al. 2010, ApJ, 724, 1524
Osterbrock, D. E. 1962, ApJ, 135, 195
Östlin, G., Bergvall, N., & Rönnback, J. 1998, A&A, 335, 85
Östlin, G., Amram, P., Bergvall, N., et al. 2001, A&A, 374, 800
Östlin, G., Zackrisson, E., Bergvall, N., & Rönnback, J. 2003, A&A, 408, 887
Östlin, G., Cumming, R. J., & Bergvall, N. 2007, A&A, 461, 471
Östlin, G., Hayes, M., Kunth, D., et al. 2009, AJ, 138, 923
Ouchi, M., Shimasaku, K., Furusawa, H., et al. 2003, ApJ, 582, 60
Ouchi, M., Shimasaku, K., Akiyama, M., et al. 2005, ApJ, 620, L1
Ouchi, M., Shimasaku, K., Furusawa, H., et al. 2010, ApJ, 723, 869
Partridge, R. B., & Peebles, P. J. E. 1967, ApJ, 147, 868
Pirzkal, N., Malhotra, S., Rhoads, J. E., & Xu, C. 2007, ApJ, 667, 49
Pritchet, C. J. 1994, PASP, 106, 1052
Prochaska, J. X., Kasen, D., & Rubin, K. 2011, ApJ, 734, 24
Rhoads, J. E., Malhotra, S., Dey, A., et al. 2000, ApJ, 545, L85
Rupke, D. S., Veilleux, S., & Sanders, D. B. 2002, ApJ, 570, 588
Sato, T., Martin, C. L., Noeske, K. G., Koo, D. C., & Lotz, J. M. 2009, ApJ, 696, 214
Scarlata, C., Colbert, J., Teplitz, H. I., et al. 2009, ApJ, 704, L98
Schwartz, C. M., & Martin, C. L. 2004, ApJ, 610, 201
Schwartz, C. M., Martin, C. L., Chandar, R., et al. 2006, ApJ, 646, 858
Shibuya, T., Kashikawa, N., Ota, K., et al. 2012, ApJ, 752, 114
Spitzer, L. 1968, Diffuse matter in space (New York: Interscience Publication)
Spitzer, L. 1978, Physical processes in the interstellar medium (Wiley Classics Library)
Vader, J. P., Frogel, J. A., Terndrup, D. M., & Heisler, C. A. 1993, AJ, 106, 1743
Verhamme, A., Schaerer, D., & Maselli, A. 2006, A&A, 460, 397
Yuma, S., Ohta, K., Yabe, K., et al. 2010, ApJ, 720, 1016
Zastrow, J., Oey, M. S., Veilleux, S., McDonald, M., & Martin, C. L. 2011, ApJ, 741, L17